Supplemental Material for: "q = 0 long-range magnetic order in centennialite CaCu₃(OD)₆Cl₂·0.6D₂O: A spin-1/2 perfect kagome antiferromagnet with J_1-J_2-J_d"

K. Iida,[1, *] H. K. Yoshida,[2] A. Nakao,[1] H. O. Jeschke,[3] Y. Iqbal,[4] K. Nakajima,[5] S. Ohira-Kawamura,[5] K. Munakata,[1]
Y. Inamura,[5] N. Murai,[5] M. Ishikado,[1] R. Kumai,[6, 7] T. Okada,[2] M. Oda,[2] K. Kakurai,[1] and M. Matsuda[8]

[1] *Neutron Science and Technology Center, Comprehensive Research
Organization for Science and Society (CROSS), Tokai, Ibaraki 319-1106, Japan*
[2] *Department of Physics, Faculty of Science, Hokkaido University, Sapporo, Hokkaido 060-0810, Japan*
[3] *Research Institute for Interdisciplinary Science, Okayama University, Okayama 700-8530, Japan*
[4] *Department of Physics, Indian Institute of Technology Madras, Chennai 600036, India*
[5] *J-PARC Center, Japan Atomic Energy Agency (JAEA), Tokai, Ibaraki 319-1195, Japan*
[6] *Institute of Materials Structure Science, High Energy Accelerator
Research Organization (KEK), Tsukuba, Ibaraki 305-0801, Japan*
[7] *Department of Materials Structure Science, The Graduate University for Advanced Studies, Tsukuba, Ibaraki 305-0801, Japan*
[8] *Quantum Condensed Matter Science Division and Shull-Wollan Center,
Oak Ridge National Laboratory, Oak Ridge, Tennessee 37831, USA*
(Dated: June 8, 2020)
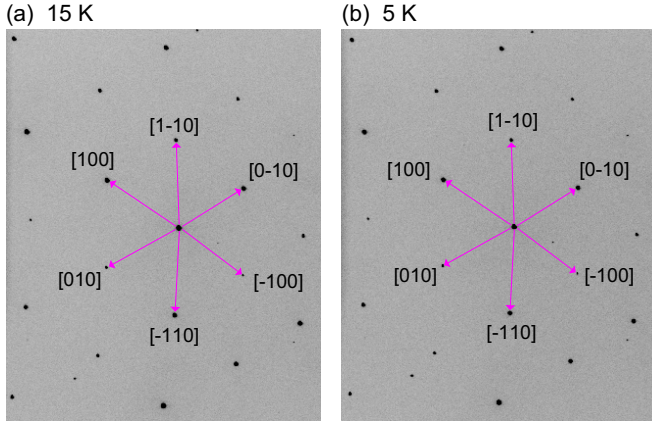
FIG. 1. X-ray diffraction spots on the imaging plates from a single-crystal CaCu₃(OH)₆Cl₂ · 0.6H₂O at (a) 15 K and (b) 5 K using BL-8A.

X-ray photographs of CaCu₃(OH)₆Cl₂ · 0.6H₂O measured at BL-8A are shown in Fig. 1. A single crystal with $0.2 \times 0.2 \times 0.1$ mm³ was mounted in the closed-cycle ⁴He cryostat. No additional peak suggesting the structural phase transition is detected upon cooling below T_N. This result indictate that both paramagnetic and antiferromagnetic phases belong to the $P\bar{3}m1$ space group. The structure refinement was done using the software ShelxL [1]. The refined crystal parameters of CaCu₃(OH)₆Cl₂ · 0.6H₂O at 5 and 15 K are summarized in Tables I and II.

Q dependences of elastic neutron scattering intensities in CaCu₃(OD)₆Cl₂ · 0.6D₂O along **Q** = $(0, K, 0.5)$ at 0.3 and 40 K are shown in Fig. 2. The magnetic Bragg peak at **Q** = $(0, 1, 0.5)$, in which the peak width is almost resolution-limited estimated by the nuclear Bragg peak at **Q** = $(0, 1, 0)$, appears at $T = 0.3$ K.

Time-of-flight neutron scattering measurements on the demnum grease were performed using the disk chopper spectrometer 4SEASONS installed at MLF, J-PARC [2,
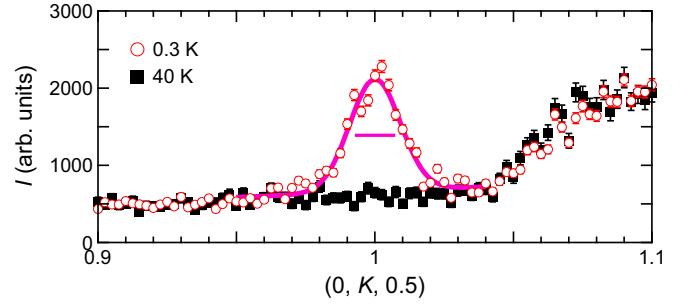
FIG. 2. **Q** dependences of elastic neutron scattering intensities in CaCu₃(OD)₆Cl₂ · 0.6D₂O along **Q** = $(0, K, 0.5)$ at 0.3 and 40 K. Horizontal bar represents the instrumental resolution estimated by the nuclear Bragg peak at **Q** = $(0, 1, 0)$ at 0.3 K.

3]. The incident energy of neutrons $E_i = 12.5$ meV with the Fermi chopper frequency of 400 Hz is used, and the energy resolution at the elastic channel is 0.43 meV (full width at half maximum). The demnum grease (DAIKIN INDUSTRIES, Ltd.) with mass of 13.6 g wrapped by the alminum foil of ∼ 3 g is measured. Elastic scattering from the demnum grease at 5 K is plotted in Fig. 3(a). $\hbar\omega$ is averaged over $[-0.2, 0.2]$ meV. Strong Bragg peak is observed at $Q = 1.31(1)$ Å⁻¹ accompanied with the broad diffuse scattering. There is also small peaks at $Q \sim 3$ Å⁻¹ in addition to the small Bragg peaks from alminum. To compare with the elastic scattering results of CaCu₃(OD)₆Cl₂ · 0.6D₂O, the elastic scattering in Fig. 3(a) is converted to the reciprocal-space map for CaCu₃(OD)₆Cl₂ · 0.6D₂O. Strong ring shape intensities corresponding to the Bragg peak at $Q = 1.31$ Å⁻¹ are observed in Fig. 3(b). We therefore concluded that the ring-shape intensities observed in the measurements for CaCu₃(OD)₆Cl₂ · 0.6D₂O in Figs. 2(a) and 2(b) in the main text are background from the demnum grease.

Single-crystal neutron diffraction results at 0.3 K us-
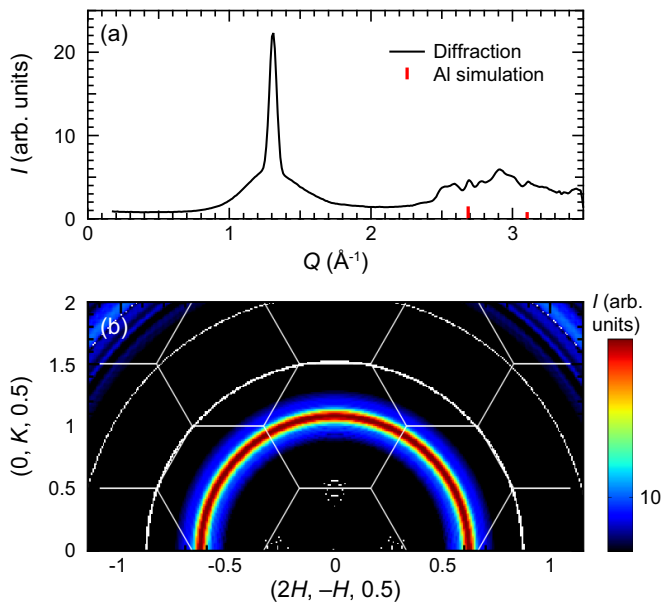
FIG. 3. (a) Elastic neutron scattering spectrum of the hydrogen-free demnum grease at 5 K with $E_i = 12.5$ meV measured at 4SEASONS. $\hbar\omega$ is averaged over $[-0.2, 0.2]$ meV. Vertical bars represent the Q positons of the Bragg peaks of aluminum. (b) Conversion of the result in panel (a) into the reciprocal-space map of $CaCu_3(OD)_6Cl_2 \cdot 0.6D_2O$. Solid lines represent the Brillouin zones of $CaCu_3(OD)_6Cl_2 \cdot 0.6D_2O$.

ing SENJU are shown in Fig. 4. A single crystal with $1.2 \times 1.2 \times 0.3$ mm^3 was mounted in the closed-cycle ^{3}He cryostat. Obtained neutron diffraction data are visualized by the STARGazer software. 36 magnetic reflections are detected. Results on magnetic structure refinements are plotted in Fig. 3 in the main text.

Fig. 5 shows temperature dependences of magnetic susceptibilities measured at $B = 1$ T under the external magnetic field directions along the ab plane and the c axis. The experimental data is taken from Ref. [4]. Solid lines show the results of the fitting by the high temperature series expansion (HTSE) [5] using the our DFT results listed in Table I in the main text as the intial parameters. The obtained parameters are $J_1 = 52.6$ K, $J_2 = 13.7$ K, and $J_d = -1.29$ K. The set of Js belongs to the $\mathbf{q} = 0$ phase in the classical phase diagram as described in Fig. 4(a) in the main text.

ADDITIONAL DFT DETAILS

We use density functional theory calculations within the full potential local orbital (FPLO) basis to study $CaCu_3(OH)_6Cl_2 \cdot 0.6H_2O$. The high space group of $P\bar{3}m1$ (No. 164) reported in Ref. [4] and Table I means that hydrogen positions of the water molecule can only be partly occupied and highly disordered. In order to perform DFT calculations, we first have to find a slightly
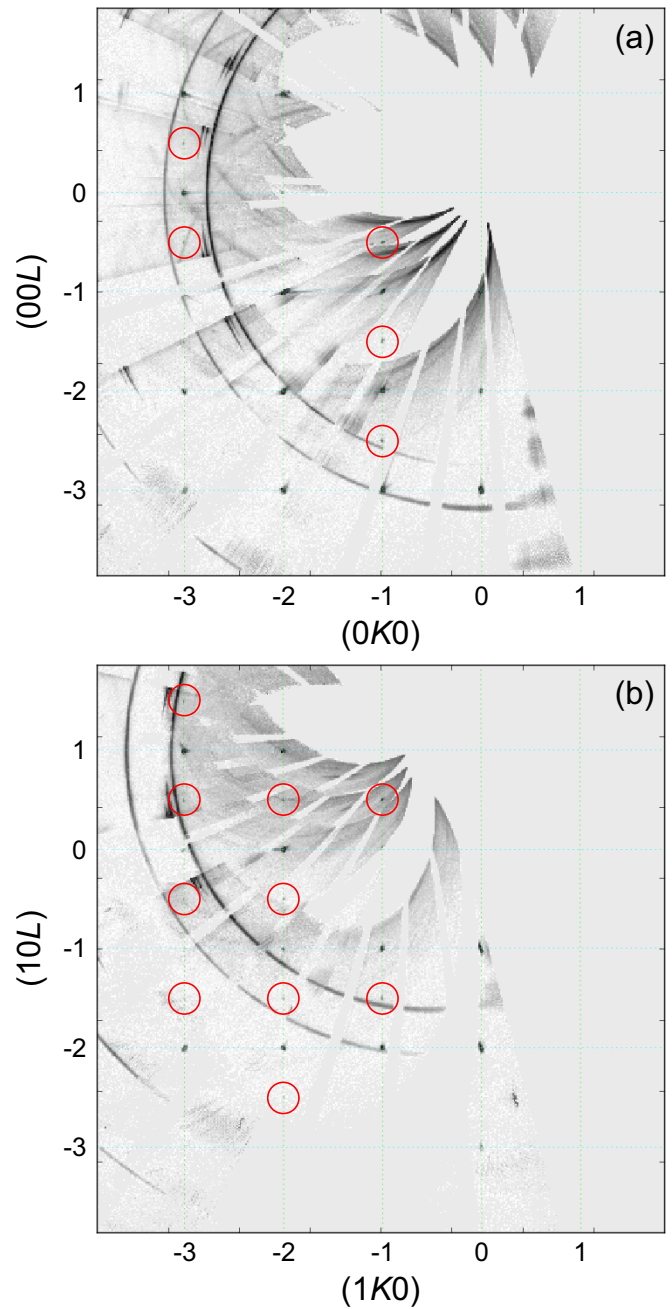
FIG. 4. Neutron diffraction intensity maps of $CaCu_3(OD)_6Cl_2 \cdot 0.6D_2O$ at 0.3 K using SENJU in (a) the $(0KL)$ plane and (b) the $(1KL)$ plane. Red circles indicate the magnetic reflections.

simplified crystal structure without partial occupation of sites. We first adopt a $\sqrt{2} \times \sqrt{2} \times 1$ supercell in which we can occupy every second water molecule position, leading to a stoichiometry of $CaCu_3(OH)_6Cl_2 \cdot 0.5H_2O$. We fix the Ca z coordinate at 0.5 with full occupancy. Furthermore, we lower the symmetry to $P2$ which allows us to add hydrogen positions to the water molecules. We then relax all hydrogen positions within DFT. It is known that the
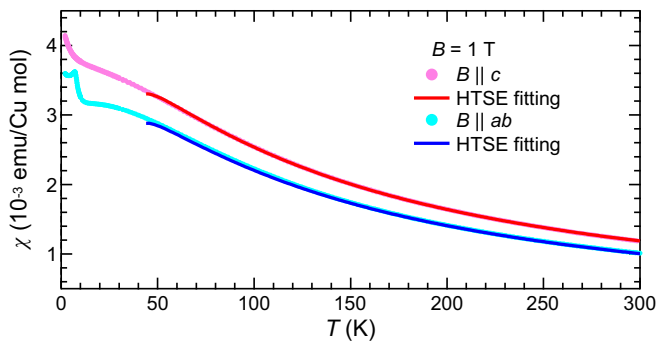
FIG. 5. Temperature dependences of magnetic susceptibilities measured at $B = 1$ T under the external magnetic field directions along the ab plane and the c axis. Solid lines show the results of the fitting by the HTSE using the our DFT results as the intial parameters.
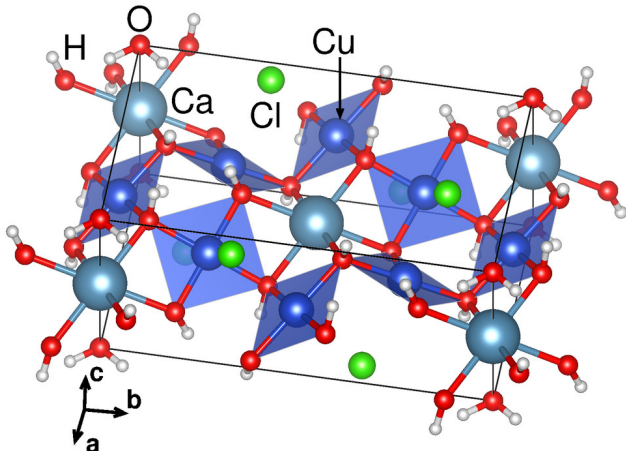
FIG. 6. Simplified structure of $CaCu_3(OH)_6Cl_2 \cdot 0.6H_2O$ which is used in the DFT calculations.

hydrogen position in the hydroxy group has an important influence on the strength of the Cu-Cu exchange [6]. The resulting structure is shown in Figure 6. We now apply the energy mapping method by calculating total energies of nine out of 216 possible spin configurations with different energy. The exchange couplings as defined

in the Heisenberg Hamiltonian of the form

$$H = \sum_{i<j} J_{ij} \, \mathbf{S}_i \cdot \mathbf{S}_j \,. \tag{1}$$

without double-counting of bonds. The fit is good [see Figure 7(d)] and yields the exchange couplings listed in Tables III and IV and shown in Figures 7(a) and 7(b). We calculate the Curie-Weiss temperature as

$$\theta_{CW} = -\frac{2}{3}S(S+1)\big(2J_1 + 2J_2 + 2J_3 + J_d\big); \tag{2}$$

where $S = 1/2$ for Cu^{2+}. The bold line in Tables III and IV indicate the interpolated U values and exchange couplings for which the Hamiltonian parameters match the measured Curie-Weiss temperature. Interestingly, the structures measured at $T = 5$ and 213 K yield virtually the same exchange couplings.

---

[1] G. M. Sheldrick, A short history of SHELX, Acta Cryst. A 64, 112 (2008).

[2] R. Kajimoto, M. Nakamura, Y. Inamura, F. Mizuno, K. Nakajima, S. Ohira-Kawamura, T. Yokoo, T. Nakatani, R. Maruyama, K. Soyama, K. Shibata, K. Suzuya, S. Sato, K. Aizawa, M. Arai, S. Wakimoto, M. Ishikado, S. Shamoto, M. Fujita, H. Hiraka, K. Ohoyama, K. Yamada, and C.-H. Lee, The Fermi Chopper Spectrometer 4SEASONS at J-PARC, J. Phys. Soc. Jpn. 80, SB025 (2011).

[3] M. Nakamura, R. Kajimoto, Y. Inamura, F. Mizuno, M. Fujita, T. Yokoo, and M. Arai, First Demonstration of Novel Method for Inelastic Neutron Scattering Measurement Utilizing Multiple Incident Energies, J. Phys. Soc. Jpn. 78, 093002 (2009).

[4] H. Yoshida, N. Noguchi, Y. Matsushita, Y. Ishii, Y. Ihara, M. Oda, H. Okabe, S. Yamashita, Y. Nakazawa, A. Takata, T. Kida, Y. Narumi, and M. Hagiwara, Unusual Magnetic State with Dual Magnetic Excitations in the Single Crystal of $S = 1/2$ Kagome Lattice Antiferromagnet $CaCu_3(OH)_6Cl_2 \cdot 0.6H_2O$, J. Phys. Soc. Jpn. 86, 033704 (2017).

[5] B. Bernu, C. Lhuillier, E. Kermarrec, F. Bert, P. Mendels, R. H. Colman, and A. S. Wills, Exchange energies of kapellasite from high-temperature series analysis of the kagome lattice J_1-J_2-J_d-Heisenberg model, Phys. Rev. B 87, 155107 (2013).

[6] Y. Iqbal, H. O. Jeschke, J. Reuter, R. Valentí, I. I. Mazin, M. Greiter, and R. Thomale, Paramagnetism in the kagome compounds $(Zn,Mg,Cd)Cu_3(OH)_6Cl_2$, Phys. Rev. B 92, 220404(R) (2015).

TABLE I. The refined crystal structure of $CaCu_3(OH)_6Cl_2 \cdot 0.6H_2O$ at 5 K using BL-8A. The space group is $P\bar{3}m1$ (No. 164), and the lattice constants are $a = b = 6.6353(2)$ Å, $c = 5.7389(7)$ Å.

Atom	Occupancy	x	y	z	U_{iso} (Å^2)	U_{11} (Å^2)	U_{22} (Å^2)	U_{33} (Å^2)	U_{23} (Å^2)	U_{13} (Å^2)	U_{12} (Å^2)
Ca	0.5	0	0	0.4445(1)	0.00575(8)	0.0019(1)	0.0019(1)	0.0134(2)	0.000	0.000	0.00095(5)
Cu	1	0.5	0.5	0.5	0.00363(5)	0.00220(5)	0.00220(5)	0.00595(7)	0.00010(1)	-0.00010(1)	0.00069(4)
Cl	1	0.6667	0.3333	0.8641(1)	0.00735(7)	0.0085(1)	0.0085(1)	0.0051(1)	0.000	0.000	0.00424(5)
O1	1	0.3810(2)	0.1905(1)	0.3564(1)	0.0087(1)	0.0104(3)	0.0071(2)	0.0098(2)	-0.0020(1)	-0.0039(2)	0.0052(1)
H	1	0.440(7)	0.223(4)	0.201(6)	0.011(8)						
O2	0.60(3)	0	0	0	0.027(2)	0.035(3)	0.035(3)	0.0094(14)	0.000	0.000	0.0176(15)

TABLE II. The refined crystal structure of $CaCu_3(OH)_6Cl_2 \cdot 0.6H_2O$ at 15 K using BL-8A. The space group is $P\bar{3}m1$ (No. 164), and the lattice constants are $a = b = 6.6383(2)$ Å, $c = 5.7416(7)$ Å.

Atom	Occupancy	x	y	z	U_{iso} (Å^2)	U_{11} (Å^2)	U_{22} (Å^2)	U_{33} (Å^2)	U_{23} (Å^2)	U_{13} (Å^2)	U_{12} (Å^2)
Ca	0.5	0	0	0.4453(1)	0.00639(8)	0.00208(9)	0.00208(9)	0.0150(2)	0.000	0.000	0.00104(5)
Cu	1	0.5	0.5	0.5	0.00377(5)	0.00215(5)	0.00215(5)	0.00645(7)	0.00008(1)	-0.00008(1)	0.00065(3)
Cl	1	0.6667	0.3333	0.8641(1)	0.00785(7)	0.00894(9)	0.00894(9)	0.0057(1)	0.000	0.000	0.00447(5)
O1	1	0.3810(2)	0.1905(1)	0.3560(1)	0.0090(1)	0.0112(3)	0.00680(1)	0.0104(2)	-0.00203(9)	-0.0041(2)	0.0056(1)
H	1	0.449(7)	0.222(4)	0.199(6)	0.019(9)						
O2	0.60(3)	0	0	0	0.027(2)	0.036(2)	0.036(2)	0.0105(12)	0.000	0.000	0.0179(12)

TABLE III. Exchange couplings of $CaCu_3(OH)_6Cl_2 \cdot 0.5H_2O$, calculated within GGA+U at $J_H = 1$ eV and $8 \times 8 \times 8$ k points for the $T = 5$ K structure. The last row contains the Cu-Cu distances which identify the exchange paths. The errors shown are only the statistical error arising from the energy mapping. The interpolated $U = 8.12$ eV set of couplings (in bold face) reproduces the experimental Curie-Weiss temperature.

U (eV)	J_1 (K)	J_2 (K)	J_3 (K)	J_d (K)	θ_{CW} (K)
6.	75.9(1.9)	3.4(1.9)	0.0(2.2)	-2.2(3.6)	-78.2
6.5	70.5(1.7)	3.0(1.7)	0.0(2.0)	-2.1(3.3)	-72.4
7.	65.4(1.6)	2.7(1.6)	0.0(1.8)	-1.9(3.0)	-67.1
7.5	60.7(1.4)	2.4(1.4)	0.0(1.6)	-1.8(2.7)	-62.2
8.	56.3(1.3)	2.2(1.3)	0.0(1.5)	-1.7(2.5)	-57.5
8.12	**55.3(1.3)**	**2.1(1.3)**	**0.0(2.5)**	**-1.6(2.5)**	**-56.5**
8.5	52.1(1.2)	1.9(1.2)	0.0(1.3)	-1.5(2.2)	-53.2
$d_{\mathrm{Cu-Cu}}$(Å)	3.31765	5.74634	6.6353	6.6353	
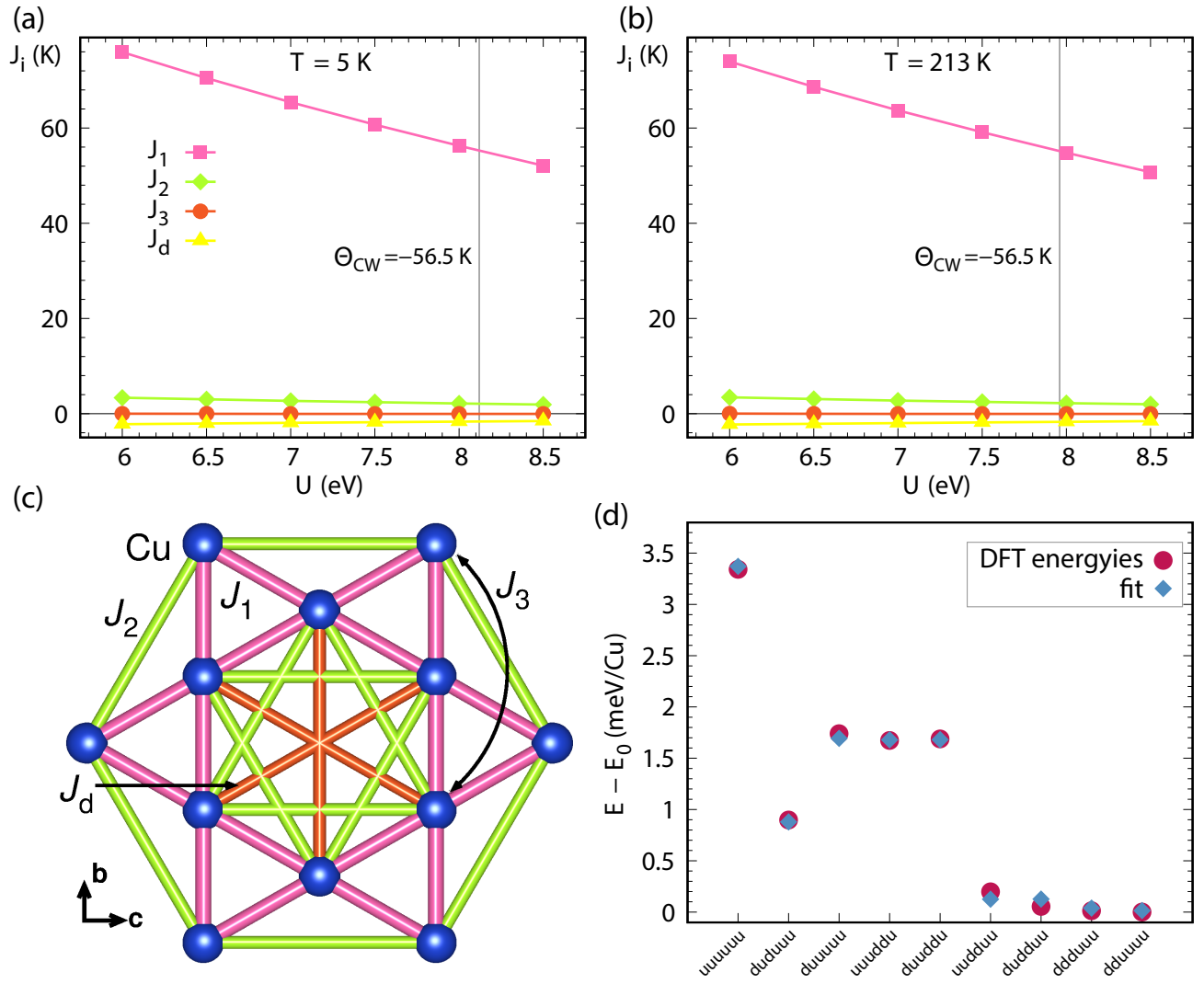
FIG. 7. Energy mapping results for $CaCu_3(OH)_6Cl_2 \cdot 0.6H_2O$. (a) and (b) Exchange couplings of $CaCu_3(OH)_6Cl_2 \cdot 0.6H_2O$ calculated with GGA+U exchange correlation functional as a function of interaction strength U and for fixed $J_H = 1$ eV for 5 K and 213 K structures, respectively. The vertical line indicates the U value at which the experimental Curie-Weiss temperature $\theta_{CW} = -56.5$ K is reproduced. The exchange paths are visualized in (c). (d) Comparison of DFT total energies with the energies calculated from the fit for $U = 8$ eV. The fit to the Heisenberg Hamiltonian is good.

TABLE IV. Exchange couplings of $CaCu_3(OH)_6Cl_2 \cdot 0.5H_2O$, calculated within GGA+U at $J_H = 1$ eV and $8 \times 8 \times 8$ k points for the $T = 213$ K structure. The last row contains the Cu-Cu distances which identify the exchange paths. The errors shown are only the statistical error arising from the energy mapping. The interpolated $U = 7.96$ eV set of couplings (in bold face) reproduces the experimental Curie-Weiss temperature.

U (eV)	J_1 (K)	J_2 (K)	J_3 (K)	J_d (K)	θ_{CW} (K)
6.	74.0(1.9)	3.4(1.9)	0.0(2.2)	-2.3(3.7)	-76.3
6.5	68.6(1.8)	3.1(1.8)	0.0(2.0)	-2.1(3.4)	-70.7
7.	63.7(1.6)	2.8(1.6)	0.0(1.8)	-2.0(3.1)	-65.5
7.5	59.1(1.5)	2.5(1.5)	0.0(1.7)	-1.8(2.8)	-60.6
7.96	**55.2(1.5)**	**2.2(1.5)**	**0.0(1.7)**	**-1.7(2.8)**	**-56.5**
8.	54.8(1.3)	2.2(1.3)	0.0(1.5)	-1.7(2.5)	-56.1
8.5	50.7(1.2)	2.0(1.2)	0.0(1.4)	-1.6(2.3)	-51.9
d_{Cu-Cu}(Å)	3.31455	5.74097	6.6291	6.6291	